

# Global Solutions of Viscous Transonic Flows in Kerr Geometry I: Weak Viscosity Limit

Sandip K. Chakrabarti

*Tata Institute Of Fundamental Research, Homi Bhabha Road, Mumbai 400005, INDIA*

Accepted . Received ; in original form

## ABSTRACT

We present fully general relativistic equations governing viscous transonic flows in vertical equilibrium in Kerr geometry. We find the complete set of global solutions (both for Optically thick and optically thin flows) in the weak viscosity limit. We show that for a large region of parameter space, centrifugal pressure supported standing shocks can form in accretion and winds very close to the black hole horizon, both for co-rotating and contra-rotating flows. We compute the nature of the shear tensor for complete transonic solutions and discuss the consequences of its reversal properties.

**Key words:** accretion, accretion disks – shock-waves – black hole physics – hydrodynamics

Appeared in MNRAS v. 283, p. 325, 1996

## 1 INTRODUCTION

The physics of accretion processes on black holes has fascinated astrophysicists for last two decades (Novikov & Thorne 1973, hereafter NT73; Lynden-Bell, 1978; Moncrief, 1980) but the full complexity of the flow behaviour is yet to be unfolded in a comprehensive manner. For example, one of the aspects that is recently studied more actively, is the accretion flow with ‘discontinuities’ or shock waves. The important numerical works of Wilson (1978) and Hawley, Smarr & Wilson (1984, 1985) show that sub-Keplerian flows experience centrifugal barrier close to the black hole and produce shock waves. Though these fully general relativistic simulations revealed the existence of only traveling shock waves, subsequent theoretical and numerical study using *pseudo-Newtonian potentials* show that shocks are indeed stationary in a large region of the parameter space (Chakrabarti, 1989 [C89]; 1990a,b [C90a],[C90b]; Molteni, Lanzafame & Chakrabarti, 1994; Sponholz & Molteni, 1994). Similarly, the formation of sub-Keplerian flows from Keplerian disks in radiation (Paczynski & Wiita, 1980) and ion pressure (Rees et al., 1982) supported disks have been shown only in the context of pseudo-Newtonian geometry (C90ab, Chakrabarti, 1996 [C96]). So far, no global solution of rotating, viscous, transonic flow (with cooling effects included) has been obtained using full general relativistic considerations. Only inviscid solutions of conical flows (with simplistic accretion rate equation) are present (C90b).

In the present paper, we derive the equations governing

the viscous transonic flows in Kerr geometry and find global solutions using the usual sonic point analysis. We present explicit examples of solutions in weak viscosity limit. We see that similar to our earlier studies using pseudo-potentials, standing shocks can form around Kerr black holes for a large range of initial flow parameters. The maximum number of sonic points remains three as was first pointed out by Liang and Thompson (1980) in the context of equatorial accretion in Schwarzschild geometry. The important difference between the present study and the earlier works (e.g., Chakrabarti 1989) is that the present work does not use pseudo-potential and therefore clearly satisfies the boundary condition on the horizon. Secondly, shock locations, particularly in prograde flows, are very close to the black hole, roughly at half as much distance as those obtained in Schwarzschild geometry. In retrograde flows, the shocks form farther away. These may have important implications in the study of hard radiations from black hole candidates (e.g., Chakrabarti & Titarchuk, 1995). Also, for the first time, the nature of shear and angular momentum transport in a viscous transonic flow just outside the black hole horizon are discussed.

In the next Section, we present the basic equations. In §3, we solve these equations in weak viscosity limit and show examples of global solutions with or without stationary shocks. In §4, we present the behavior of shear tensor which is responsible for angular momentum transport. Finally, in §5, we make concluding remarks.

## 2 BASIC EQUATIONS

We use  $t$ ,  $r$ ,  $\theta$  and  $z$  as the coordinates. We choose the geometric units where  $G = M_{bh} = c = 1$  ( $G$  is the gravitational constant,  $M_{bh}$  is the mass of a black hole and  $c$  is the velocity of light). We also consider  $|\theta - \pi/2| \ll 1$  for a thin flow in vertical equilibrium. We consider a perfect fluid with the stress-energy tensor,

$$T_{\mu\nu} = \rho u_\mu u_\nu + p(g_{\mu\nu} + u_\mu u_\nu) \quad (1)$$

where,  $p$  is the pressure and  $\rho = \rho_0(1+\pi)$  is the mass density,  $\pi$  being the internal energy. We ignore the self-gravity of the flow. We assume the vacuum metric around a Kerr black hole to be of the form (e.g., NT73),

$$ds^2 = g_{\mu\nu} dx^\mu dx^\nu = -\frac{r^2 \Delta}{A} dt^2 + \frac{A}{r^2} (d\phi - \omega dt)^2 + \frac{r^2}{\Delta} dr^2 + dz^2 \quad (2)$$

Where,

$$A = r^4 + r^2 a^2 + 2ra^2$$

$$\Delta = r^2 - 2r + a^2$$

$$\omega = \frac{2ar}{A}$$

Here,  $g_{\mu\nu}$  is the metric coefficient and  $u_\mu$  is the four velocity components:

$$u_t = \left[ \frac{\Delta}{(1-V^2)(1-\Omega)(g_{\phi\phi} + l g_{t\phi})} \right]^{1/2} \quad (3a)$$

and

$$u_\phi = -l u_t \quad (3b)$$

where, the angular velocity is

$$\Omega = \frac{u^\phi}{u^t} = -\frac{g_{t\phi} + l g_{tt}}{g_{\phi\phi} + l g_{t\phi}} \quad (4)$$

and  $l$  is the specific angular momentum. The radial velocity  $V$  in the rotating frame is (C90b, p. 137)

$$V = \frac{v}{(1-\Omega l)^{1/2}}$$

where,

$$v = \left( -\frac{u_r u^r}{u_t u^t} \right)^{1/2}.$$

Since  $V = 1$  on the horizon and even in the extreme equation of state of  $p = \rho/3$ , the flow must be supersonic on the horizon. Thus, *any black hole accretion is necessarily transonic* (also, see C90b).

### 2.1 Equations Governing a Viscous Transonic Flow

In the present paper, we shall concentrate on the time independent solutions of the underlying hydrodynamic equations. The equation for the balance of the radial momentum is obtained from  $(u_\mu u_\nu + g_{\mu\nu})T_{;\nu}^{\mu\nu} = 0$ :

$$\vartheta \frac{d\vartheta}{dr} + \frac{1}{r\Delta} [a^2 - r + \frac{A\gamma^2 B}{r^3}] \vartheta^2 + \frac{A\gamma^2}{r^6} B + \left( \frac{\Delta}{r^2} + \vartheta^2 \right) \frac{1}{p + \rho} \frac{dp}{dr} = 0 \quad (5)$$

where,

$$\gamma^2 = \left[ 1 - \frac{A^2}{\Delta r^4} (\Omega - \omega) \right]^{-1},$$

$$B = (\Omega a - 1)^2 - \Omega^2 r^3,$$

and

$$\vartheta = u^r.$$

Here and hereafter we use a comma to denote an ordinary derivative and a semi-colon to denote a covariant derivative. The baryon number conservation equation (continuity equation) is obtained from  $(\rho_0 u^\mu)_{;\mu} = 0$  which is,

$$\dot{M} = 2\pi r \vartheta \Sigma = 2\pi r \vartheta \rho_0 H_0 \quad (6)$$

where,

$$H_0 = \left( \frac{p}{\rho_0} \right)^{1/2} \frac{r^{3/2}}{\gamma} \left[ \frac{(r^2 + a^2)^2 - \Delta a^2}{(r^2 + a^2)^2 + 2\Delta a^2} \right]^{1/2}$$

is the height of the disk in vertical equilibrium (NT73). The equation of the conservation of angular momentum is obtained from  $(\delta_\phi^\mu T^{\mu\nu})_{;\nu} = 0$ , and one obtains,

$$\rho_0 u^\mu (h u_\phi)_{;\mu} = (\eta \sigma_\phi^\gamma)_{;\gamma}$$

where,

$$\eta = \nu \rho_0$$

is the coefficient of dynamical viscosity and  $\nu$  is the coefficient of kinematic viscosity. When rotation is dominant ( $\vartheta < u^\phi$ ) the relevant shear tensor component  $\sigma_\phi^r$  is given by (Anderson & Lemos, 1988),

$$\sigma_\phi^r = -\frac{A^{3/2} \gamma^3 \Omega_{,r} \Delta^{1/2}}{2r^5} \quad (7)$$

so that the angular momentum equation takes the form,

$$\mathcal{L} - \mathcal{L}_+ = -\frac{1}{\vartheta r^5} \frac{d\Omega}{dr} \nu A^{3/2} \gamma^3 \Delta^{1/2}. \quad (8)$$

Here we have modified earlier work of NT73 and Peitz (1994) in that the fluid angular momentum  $\mathcal{L} = -h u_\phi$ , rather than particle angular momentum  $-u_\phi$  is used. That way, for an inviscid flow ( $\eta = 0$ ) one recovers  $\mathcal{L} = \text{constant}$  as in a fluid picture. Similarly, the radial velocity term is included (eq. 3) and angular momentum is allowed to be non-Keplerian (eq. 8).  $\mathcal{L}_+$  is the angular momentum on the horizon since the *rotational* shear (as defined by eq. 7) vanishes there. In presence of significant radial velocity, the shear in eq. (7) is to be replaced by its full expression,  $\sigma^{\mu\nu} = (u_{;\beta}^\mu P^{\beta\nu} + u_{;\beta}^\nu P^{\beta\mu})/2 - \Theta P^{\mu\nu}/3$  where  $P^{\mu\nu} = g^{\mu\nu} + u^\mu u^\nu$  is the projection tensor and  $\Theta = u^\mu_{;\mu}$  is the expansion (e.g., Shapiro & Teukolsky, 1983) which no longer vanishes on the horizon (see, Fig. 6 below). In that case,  $\mathcal{L}_+$  will no longer be the specific angular momentum of the flow at the horizon, instead it will be at the place where the net shear effect vanishes. In Section 4, we shall compare these shear components in a realistic solution.

Entropy generation equation is obtained from the first law of thermodynamics along with the baryon conservation equation  $(S^\mu)_{;\mu} = [2\eta \sigma_{\mu\nu} \sigma^{\mu\nu}]/T - Q^-$ :

$$\vartheta \Sigma \left( \frac{dh}{dr} - \frac{1}{\rho_0} \frac{dp}{dr} \right) = Q^+ - Q^- = 2\nu \Sigma \sigma_{\mu\nu} \sigma^{\mu\nu} - Q^-$$

where  $Q^+$  and  $Q^-$  are the heat generation rate and the heat loss rate respectively.  $h$  is the specific enthalpy:  $h = (p + \rho)/\rho_0$ . Here, we ignore the terms contributed by radiation. Using rotational shear as given in eq. (7), the entropy equation takes the form,

$$\vartheta\Sigma\left(\frac{dh}{dr} - \frac{1}{\rho_0}\frac{dp}{dr}\right) = \frac{\nu\Sigma A^2\gamma^4(\Omega,r)^2}{r^6} - Q^-. \quad (9)$$

Of course, for accuracy, we use the full expression for  $\sigma_\phi^r$  as discussed above.

This set of equations are solved simultaneously keeping in mind that the shock waves may form in the flow, where, the following momentum balance condition

$$W_-n^\nu + (W_- + \Sigma_{0-})(u_-^\mu n_\mu)u_-^\nu = W_+n^\nu + (W_+ + \Sigma_{0+})(u_+^\mu n_\mu)u_+^\nu \quad (10)$$

along with the conservation of energy and mass fluxes (together, these conditions are known as the Rankine-Hugoniot conditions) must be fulfilled. Here,  $n_\mu$  is the four normal vector component across the shock, and  $W$  and  $\Sigma$  are vertically integrated pressure and density on the shock surface. The subscripts  $-$  and  $+$  denote the pre-shock and post-shock quantities respectively.

The equations presented above are applicable to optically thin as well as optically thick flows for any general heating and cooling processes. For a given viscosity prescription and the exact cooling processes (depending on the optical depth of the flow), it is usual to reduce the above set of equations in the form (Bondi, 1952):

$$\frac{du}{dr} = \frac{N}{D} \quad (11)$$

where  $N$  and  $D$  are the smooth functions of radial coordinate (unless there are non-linearities which prevent such reduction. In that case sonic curve analysis is done, see Flammang, 1982). The procedure of obtaining the complete solution is then similar to what is presented in obtaining the global solutions of viscous transonic flow using pseudo-Newtonian potential (C90a,b; C96 and references therein). Presently, we concentrate on the solution of the above set of equations in the inviscid limit. Full discussion on strongly viscous flows will be presented elsewhere.

## 2.2 Sonic Point Conditions in Weak Viscosity Limit

In the case when viscosity is negligible, equations (5) and (8) could be integrated to obtain the energy and angular momentum conservation equations (Moncrief, 1980; Flammang, 1982; C90b),

$$hu_t = \frac{p + \rho}{\rho_0}u_t = \mathcal{E}, \quad (12a)$$

and

$$hu_\phi = \frac{p + \rho}{\rho_0}u_\phi = -\mathcal{L}. \quad (12b)$$

From eq. (6) we get the constant accretion rate as,

$$\dot{M} = 2\pi r\vartheta\rho_0 H_0. \quad (12c)$$

In the weak viscosity limit, the entropy equation (9) can be replaced by an adiabatic equation of state  $P = K\rho_0^{1+1/n}$ .  $K$ , which is a measure of entropy, is constant in the flow

but it changes at the shocks (the entropy generated may be either radiated or advected away depending on the cooling efficiency of the flow at the shock; see C90b),  $n$  is the polytropic index related to the adiabatic index  $\Gamma$  by  $\Gamma = 1 + 1/n$ , and is assumed to be constant throughout the flow. The specific enthalpy and the density in terms of the sound speed  $a_s = (\partial P/\partial\rho)^{1/2}$  become,

$$h = \frac{1}{1 - na_s^2} \quad (13a)$$

$$\rho_0 = \left[\frac{na_s^2}{K(n+1)(1 - na_s^2)}\right]^n \quad (13b)$$

First we rewrite the energy and mass conservation equations on the equatorial plane as ( $\theta = \pi/2$ ),

$$\mathcal{E} = \frac{1}{1 - na_s^2} \frac{1}{(1 - V^2)^{1/2}} \left(\frac{\Delta}{D}\right)^{1/2} \quad (14a)$$

and

$$\dot{M} = \left(\frac{a_s^2}{1 - na_s^2}\right)^{n+1/2} \frac{V}{(1 - V^2)^{1/2}} \left[\frac{\Delta r^3 \{(r^2 + a^2)^2 - \Delta a^2\}}{\gamma \{(r^2 + a^2)^2 + 2\Delta a^2\}}\right]^{1/2} \quad (14b)$$

where,

$$D = (1 - \Omega l)(g_{\phi\phi} + lg_{t\phi}) = r^2 + \frac{2l^2}{r}\left(1 - \frac{a}{l}\right)^2 - l^2\left(1 - \frac{a^2}{l^2}\right). \quad (15a)$$

$$v_\phi = \left(-\frac{u_\phi u^\phi}{u_t u^t}\right)^{1/2}. \quad (15b)$$

The quantity  $\dot{M}$  will be called the *entropy accretion rate* as  $\dot{M} \propto K^n \dot{M}$ . It usually assumes two different values at two saddle type sonic points and the one with the smallest  $\dot{M}$  joins horizon with infinity (C89, C90b). This quantity, which is very useful in the study of shocks, was defined for the first time in C89 and was simply termed as ‘accretion rate’. In presence of an accretion shock, the transonic flow passes through both the sonic points.

Differentiating equations (14a) and (14b), and eliminating terms involving derivatives of  $a_s$ , we obtain,

$$\frac{dV}{dr} = \frac{N}{D} = \frac{c_1 a_2 - c_2 a_1}{b_1 a_2 - b_2 a_1} \quad (16)$$

where,

$$a_1 = \frac{2na_s}{1 - na_s^2} \quad (17a)$$

$$a_2 = \frac{2n + 1}{a_s(1 - na_s^2)} \quad (17b)$$

$$b_1 = \frac{V}{1 - V^2} \quad (17c)$$

$$b_2 = \frac{1}{V(1 - V^2)} \quad (17d)$$

$$c_1 = \frac{r - 1}{\Delta} - \frac{r - \frac{l^2}{r^2}(1 - \frac{a}{l})^2}{D} \quad (17e)$$

$$c_2 = \frac{3}{2r} + \frac{r - 1}{\Delta} - \frac{\gamma'}{\gamma} + \frac{H_0'}{H_0} \quad (17f)$$

Where a prime ( $'$ ) denotes ordinary derivative with respect to  $r$ . From the vanishing condition of  $N$  and  $D$  at the sonic points, one obtains the so called sonic point conditions as,

$$V_c^2 = \frac{c_1}{c_2} \Big|_c \quad (18a)$$

and

$$a_{s,c} = V_c \left( \frac{2n+1}{2n} \right)^{1/2} \quad (18b)$$

Here, the subscript 'c' refers to the quantities evaluated at the sonic point  $r = c$ . The sonic point condition (7b) implies a Mach number  $M = V/a_s = (2n/2n+1)^{1/2}$  at the sonic point. This is of the same form as the flow in vertical equilibrium in pseudo-Newtonian potential (C89), though the velocities here are defined with relativistic corrections. In conical flows in Kerr geometry (with a simpler accretion rate equation),  $M = 1$  at the sonic point (C90b).

In obtaining a global solution one supplies the conserved quantities at the inner (such as the disk surface) or the outer (e.g. Keplerian or sub-Keplerian flows injected at the outer region) boundary, depending upon whether one is interested in the wind solution or the accretion solution. For a given angular momentum  $l$ , the remaining unknowns are  $V(r)$ ,  $a_s(r)$ . But one requires only one extra boundary condition, e.g.,  $\mathcal{E}$ , since two sonic point conditions (eqs. 18a and 18b) introduce only one extra unknown, namely,  $r_c$ . Thus, the supply of the initial specific energy  $\mathcal{E}$  and the specific angular momentum  $l$  are sufficient for a complete solution from the horizon to infinity. For a viscous flow, one clearly has to supply the distribution of viscosity  $\eta(r)$  (e.g., ion or magnetic viscosity) itself. Simple Shakura & Sunyaev (1973) viscosity prescription may not be very useful since that stress  $-\alpha P$  is always negative, while in a general relativistic flow stress can change signs. Note that by definition,  $\Omega = \omega$  on the horizon and thus the flow co-rotates with the black hole. Instead of specifying various quantities at the flow boundary, one can alternatively specify the location of a critical point along with the energy or the angular momentum as in C90a,b.

In much of the parameter space, the flow is expected to be smooth as in a Bondi flow. However, if the angular momentum is significant, matter can pile up behind the centrifugal barrier close to the black hole and form a standing shock wave. At the shock, apart from the continuity of the energy and mass flux, the relativistic momentum balance condition (eq. 10) must be satisfied. Using Newtonian definition of the vertical integration (since we are dealing with thin flows anyway) as in C89 and the definition of entropy accretion rate  $\dot{\mathcal{M}}$ , we find that at the shock, the following quantity:

$$\Pi = \frac{\left[ \frac{a_s^2}{1 - n a_s^2} \right]^{n+3/2} \left( \frac{2}{3\Gamma-1} + \frac{V^2}{a_s^2(1-V^2)} \right)}{\dot{\mathcal{M}}} \quad (19)$$

should be continuous. One can use different prescriptions, but the general behaviour is not expected to change.

### 3 BEHAVIOUR OF SONIC POINTS AND GLOBAL SOLUTIONS

Before obtaining a globally complete solution, we can make a general study of the sonic point behaviour of a weakly vis-

cous flow. Using eq. 14a, eq. 18a and eq. 18b, we can compute the specific energy  $\mathcal{E}$  of the flow (which is conserved) as a function of the sonic radius  $r_c$  and specific angular momentum of the flow. Figs. 1(a-b) shows our findings for  $a = 0.95$ . We choose  $\Gamma = 4/3$ , i.e.,  $n = 3$ . In Fig. 1a, from the top curve to the bottom we use,  $l = 2.0, 2.1, 2.2, 2.3, 2.4$  and  $2.5$ . The number of sonic points of the flow for a given energy and angular momentum will depend on the number of intersections between a  $\mathcal{E} = \text{constant}$  line and a constant angular momentum curve. If the slope of the curve is negative the sonic point is saddle type and is physical, otherwise it is of circle type or 'O' type (see, C89, C90a,b) which is unphysical and irrelevant. We note that for a very high energy  $\mathcal{E} \gg 1$  or for low angular momentum there is only one saddle type sonic point as in Bondi accretion (Bondi, 1952). But near  $\mathcal{E} = 1$  (i.e., the rest mass), there could be three sonic points (see Fig. 3 below). The innermost and the outermost intersections represent saddle type sonic points and the middle intersection represents the 'O' type sonic point. For low angular momentum (say, for  $l = 2.0$ ) there is only one sonic point for all energy with which matter enters the black hole. This is similar to a spherical Bondi flow. However, for higher angular momentum, say  $l = 2.3$ , there could be two saddle type sonic points for a range of energy. The presence of the second saddle type point is the general relativistic effect, as discussed in C90b or C96. In Fig. 1b, we present results for retrograde flows with angular momenta (from the top curve to the bottom),  $l = 3.4, 3.8, 4.2, 4.6, 5.0$  and  $5.4$ . Here, to have three sonic points the flow requires a larger angular momentum. This is because the matter has to fight against the frame-dragging effects which forces the flow to co-rotate with the horizon. The terms containing  $a/l$  in Eq. (15a) and Eq. (17e) represent the coupling of the spin angular momentum of the black hole and the orbital angular momentum of the particle which bring about this change of behaviour. In either cases, however, the flow angular momentum that we consider here are around marginally stable value or even less. Thus, they are not high in any real sense.

For a higher polytropic index, say, for  $\Gamma = 5/3$ , the number of saddle type sonic points is only one. The  $\Gamma = \Gamma_{crit}$  at which the transition from two saddle type points to just one saddle type sonic point takes place depends on the geometry of the flow. Typically, we find that for a flow in vertical equilibrium,  $\Gamma_{crit} \sim 1.5$  (see also, C90b; C96).

Another important property of the flow which could be studied before solving the full set of equations is the dependence of entropy accretion rate on specific energy at various sonic points for a given angular momentum of the flow. Since one requires only two free parameters for a global solution, when a pair  $(\mathcal{E}, l)$  is supplied at the outer boundary,  $\dot{\mathcal{M}}$  must be regarded as an eigenvalue of the problem. Note that only the product of entropy function  $K^n$  and the mass accretion rate  $\dot{M}$  is determined by the boundary condition, not the individual quantities. Thus, a specific flow property, such as shock location, could be completely independent of the mass flux  $\dot{M}$ . When cooling processes (which depend on mass accretion rate) are used, the result will depend on accretion rates, except when cooling relation is simple (such as  $Q^-/Q^+ = \text{constant}$ , see C96).

In Fig. 2, we present the variation of the specific energy  $\mathcal{E}$  with entropy accretion rate  $\dot{\mathcal{M}}$  as the sonic point is changed. This is for inviscid flow ( $\eta(r) = 0$ ). The direction

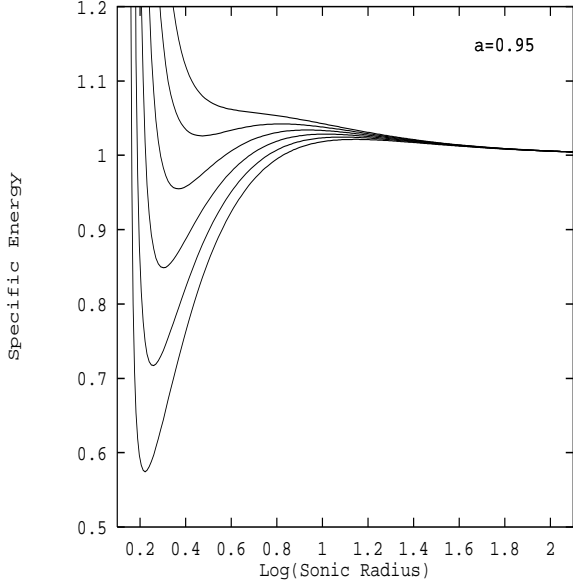


**Fig. 1a:** Plot of specific energy  $\mathcal{E}$  as functions of the sonic point ( $x_c$ ) for  $l = 2.0, 2.1, 2.2, 2.3, 2.4$  and  $2.5$  (from top to bottom).  $a = 0.95$  is used. For some range of energy, the curves of certain  $l$  may have three intersections, signifying the presence of three sonic points and possibility of shock waves.

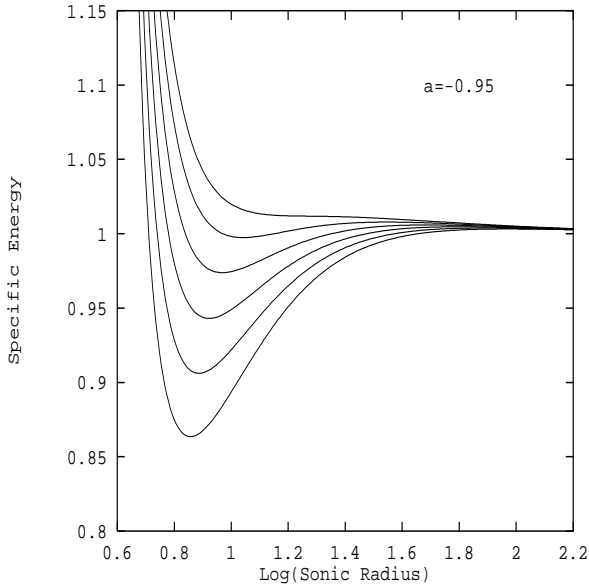


**Fig. 1b:** Same as (a) but for contra-rotating flow with  $l = 3.4, 3.8, 4.2, 4.6, 5.0$  and  $5.4$  (from top to bottom). The sonic points are located farther out in this case.

of the arrow on the curve indicates the direction in which the sonic point is increased. The specific angular momentum of the flow is  $l = 2.3$  and  $a = 0.95$  is chosen as before. The branches  $AMB$  and  $CMD$  are drawn for the inner and the outer sonic points respectively and the branch  $BC$  is drawn for the circle type sonic point (C89). For a given mass accretion rate  $\dot{M}$ , the entropy accretion rate measures the specific entropy of the flow. In the energy range spanned by  $MC$ ,  $\dot{M}_o > \dot{M}_i$ , and in the energy range spanned by  $MD$ ,  $\dot{M}_o < \dot{M}_i$ . (Here, the subscripts  $i$  and  $o$  denote the quantities at the inner and the outer sonic points respectively.)

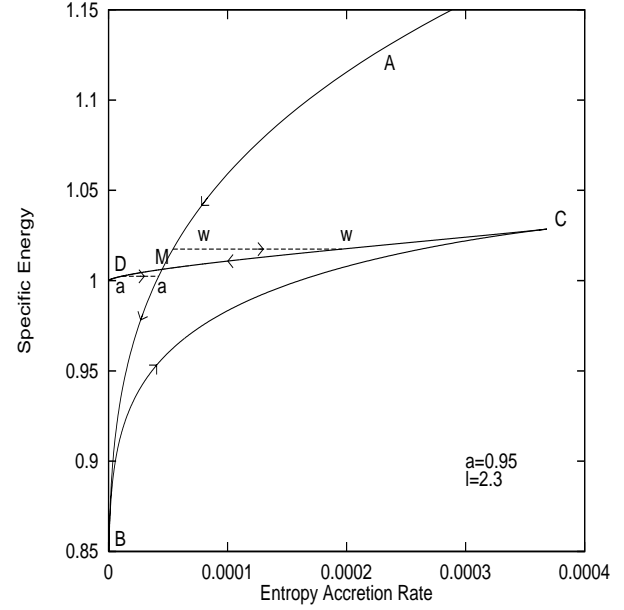


**Fig. 2:** Plot of specific energy  $\mathcal{E}$  against the entropy accretion rate  $\dot{M}$  at all the sonic points of the flow of angular momentum  $l = 2.3$  around a Kerr black hole of  $a = 0.95$ . Sections  $AMB$  and  $CMD$  denote results on inner and outer saddle type sonic points respectively, and the section  $BC$  denotes results of center type sonic point. Horizontal arrows  $aa$ , and  $ww$  schematically show shock transitions in accretion and winds respectively. Arrows on the curves show the direction in which the sonic point is increased.

However, since only smaller of the two  $\dot{M}$ s joins the flow at infinity (C90b), only allowed (shock free) flow must have parameters either on  $AM$  (accretion or wind through inner sonic point) or on  $MD$  (accretion or wind through outer sonic point). In some regions of the parameter space close to  $M$ , two different transonic flows (e.g., two flows with the same energy and angular momentum, but different entropy accretion rate) can be ‘glued’ together through shock conditions. For example, a flow, first passing through an outer sonic point on  $MD$  can undergo a shock  $aa$  and generate enough entropy to ‘land on’ the branch  $MB$  so that it can now pass through the inner sonic point. This is an example of the accretion shock. We shall show this solution in Fig. 3 below. Conversely, a wind flow can first pass through an inner sonic point on  $MA$  and after passing through a shock can land on a point on the branch  $MC$  so that it can pass through the outer sonic point also. This solution is also shown in Fig. 3 below. In order to have a shock, of course,  $\Pi$  of Eq. (9) must be continuous across the shock (that defines ‘some’ region of energy close to the point  $M$  on the curve.).

So far, we discussed the nature of solutions when both the saddle type sonic points are present. This is true only in an energy range  $\Delta\mathcal{E}$  spanned by the curve  $CMD$  (see, Fig. 3 below). Otherwise, the flow will have only one saddle type sonic point, and it will surely not have a standing shock wave of the kind we are discussing here (though shocks by external irradiation which forces the flow to be subsonic cannot be ruled out). The whole range of  $\Delta\mathcal{E}$  does not allow shock solution, but only a part, in which Rankine-Hugoniot condition is satisfied, is allowed. This will be shown below.

In Fig. 3 we classified the *entire* parameter space according to the type of inviscid solutions that is prevalent.

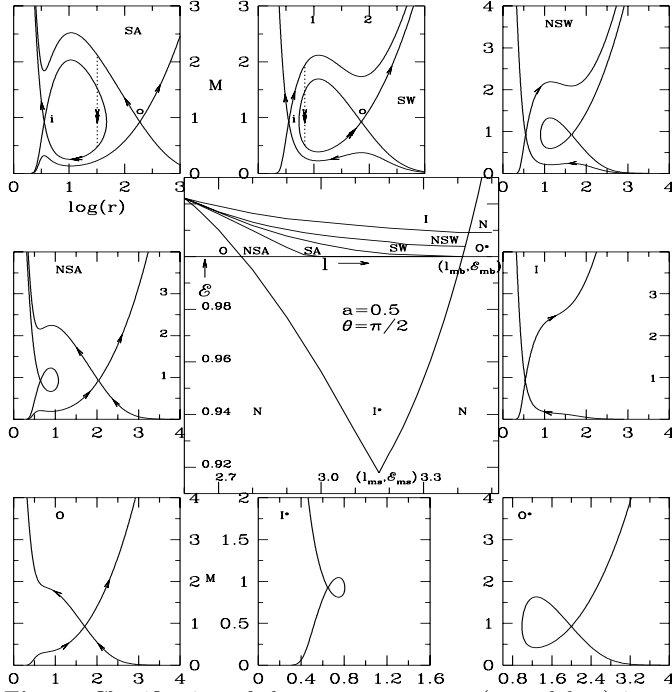


**Fig. 3:** Classification of the parameter space (central box) in the energy-angular momentum plane in terms of various topology of the black hole accretion. Eight surrounding boxes show the solutions from each of the independent regions of the parameter space. Each small box shows Mach number  $M$  against the logarithmic radial distance  $r$ . Contours are of constant entropy accretion rate  $\dot{M}$ . Parameters from region  $N$  does not form any transonic solution. See text for details.

We choose  $a = 0.5$ . (For classification of flows in pseudo-Newtonian geometry, see C89, C90ab). The adiabatic index  $\Gamma = 4/3$  has been chosen. In the central box, we divide the parameter space spanned by  $(l, \mathcal{E})$  into nine regions marked by  $N, O, NSA, SA, SW, NSW, I, O^*, I^*$ . The horizontal line at  $\mathcal{E} = 1$  corresponds to the rest mass of the flow. Surrounding this parameter space, we plot various solutions (Mach number  $M = v_r/a_s$  vs. logarithmic radial distance where  $v_r$  is the radial velocity and  $a_s$  is the sound speed) marked with the same notations (except  $N$ ). Each of these solution topologies has been drawn using flow parameters from the respective region of the central box. The accretion solutions have inward pointing arrows and the wind solutions have outward pointing arrows. The crossing points are ‘X’ type or saddle type sonic points and the contours of circular topology are around ‘O’ type sonic points. If there are two ‘X’ type sonic points, the inner one is called the inner sonic point and the outer one is called the outer sonic point. If there is only one ‘X’ type sonic point in the entire solution, then the terminology of inner or outer is used according to whether the sonic point is closer to or farther away from the black hole. The solutions from the region ‘O’ has only the outer sonic point. The solutions from the regions  $NSA$  and  $SA$  have two ‘X’ type sonic points with the entropy density  $S_o$  at the outer sonic point less than the entropy density  $S_i$  at the inner sonic point. However, flows from  $SA$  pass through a standing shock since the Rankine-Hugoniot condition is satisfied. The entropy generated at the shock  $S_i - S_o$  is advected towards the black hole to enable the flow to pass through the inner sonic point. Rankine-Hugoniot condition

is not satisfied for flows from the region  $NSA$ . Numerical simulations show (Ryu, Chakrabarti & Molteni, 1997) that the flow from this region is very unstable and exhibit periodic changes in emission properties as the flow constantly tries to form the shock wave, but fails to do so. The solutions from the region  $SW$  and  $NSW$  are very similar to those from  $SA$  and  $NSA$ . However,  $S_o \geq S_i$  in these cases. Shocks can form only in winds from the region  $SW$ . The shock condition is not satisfied in winds from the region  $NSW$ . This may make the  $NSW$  flow unstable as well. A flow from region  $I$  only has the inner sonic point and thus can form shocks (which require the presence of two saddle type sonic points) only if the inflow is already supersonic due to some other physical processes. Each solution from regions  $I^*$  and  $O^*$  has two sonic points (one ‘X’ and one ‘O’) only and neither produces complete and global solution. The region  $I^*$  has an inner sonic point but the solution does not extend subsonically to a large distance. The region  $O^*$  has an outer sonic point, but the solution does not extend supersonically to the horizon! When a significant viscosity is added, the closed topology of  $I^*$  opens up as described in C90ab and C96, and the flow may join with a cool Keplerian disk with  $\mathcal{E} < 1$ . These special solutions of viscous transonic flows should not have centrifugally supported shock waves as they have only one inner sonic point. However, hot flows deviating from a Keplerian disk or, sub-Keplerian winds from companions or, cool flows subsequently energized by magnetic flares (for instance) will have  $\mathcal{E} > 1$  and thus could have standing or periodically varying shock waves as discussed above. The post-shock flow radiates most of the observed hard radiation as shown by Chakrabarti & Titarchuk (1995). Note that parameters from region  $N$  does not produce any transonic solution.

In C89 and C90ab, it was found that shock conditions were satisfied at four locations:  $r_{s1}, r_{s2}, r_{s3}, r_{s4}$ , though  $r_{s1}$  and  $r_{s4}$  were found to be not useful for accretion on black holes. Out of  $r_{s2}$  and  $r_{s3}$ , it was shown that  $r_{s3}$  is stable for accretion flow and  $r_{s2}$  is stable for winds (Chakrabarti & Molteni, 1993, also see, Nakayama, 1994 and Nobuta & Hanawa, 1994). We plot here only  $r_{s3}$  here in  $SA$  and  $r_{s2}$  in  $SW$  solutions. Here,  $o$  and  $i$  are the outer and inner sonic points respectively. In the box containing a solution from  $SA$ , we chose  $a = 0.5, l = 3, \mathcal{E} = 1.003$ . For these parameters, the eigenvalue of the critical entropy accretion rates at the two saddle type sonic points are  $\dot{M}_i = 2.74 \times 10^{-5}$  and  $\dot{M}_o = 1.491 \times 10^{-5}$  respectively. Here,  $\dot{M}_o < \dot{M}_i$ , hence the flow through the outer sonic point joins the horizon with infinity (single arrowed curve). The flow forms a shock and jump onto the branch which passes through  $i$  as shown by double arrows. The stable shock (shown by a vertical dashed line) is located at  $a_3 = r_{s3} = 32.29$  (in C89 notation). Only this jump, namely, a generation of entropy of amount  $\dot{M}_i - \dot{M}_o$  is allowed in order that the transonicity of the post-shock flow is guaranteed. The entropy generated at the shock is advected through the inner sonic point. The flow is inefficiently cooled, which keeps the energy of the flow constant. This makes the flow much hotter than a Keplerian disk. (This is typical of advective disks. See, C89, C96.) In  $SW$  solution, we chose  $a = 0.5, l = 3, \mathcal{E} = 1.007$ . For these parameters, the eigenvalue of the critical entropy accretion rates at the two saddle type sonic points are  $\dot{M}_i = 3.12 \times 10^{-5}$  and  $\dot{M}_o = 5.001 \times 10^{-5}$  re-

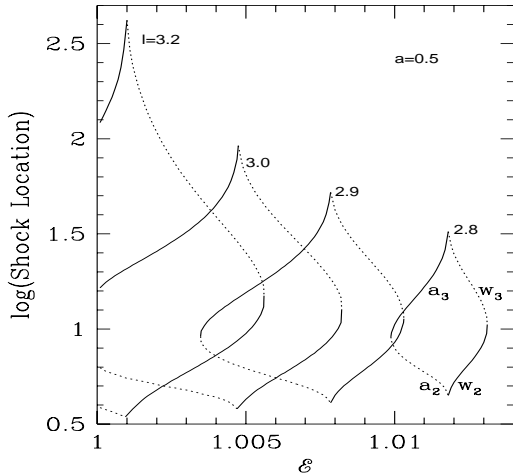


**Fig. 4:** Variation of shock locations with energy in accretion and winds for various specific angular momenta  $l$  (marked on curves).  $a = 0.5$  is chosen. Segments marked  $a_3$  and  $w_2$  (solid curves) represent stable shocks in accretion and winds respectively. Other two segments ( $a_2$  and  $w_3$ ) represent formal shock locations which are unstable.

spectively. Here,  $\dot{M}_i < \dot{M}_o$ , hence the flow through the inner sonic point  $i$  joins the horizon with infinity (single arrowed curve). The accretion flow can no longer form a shock. But a wind, first passing through  $i$  can, as shown in double arrows. The stable shock (shown by a vertical dashed line) is located at  $w_2 = r_{s2} = 6.89$  in this case. Only this jump, namely, a generation of entropy of amount  $\dot{M}_o - \dot{M}_i$  is allowed at the shock in order that it can escape to infinity through the outer sonic point  $O$ . This consideration, along with the continuity of  $\Pi$  (Eq. 19) allows one to locate stationary shock waves in a flow. Note that though the flow has a shock-free solution (passing through  $o$  for accretion in  $SA$  solution and through  $i$  for winds in  $SW$  solution in Fig. 3), the flow would choose to pass through a shock because the latter solution is of higher entropy. This fact has been verified through numerical simulations of accretion and wind flows (Chakrabarti & Molteni, 1993; Molteni, Lanzafame & Chakrabarti, 1994). It is to be noted that the angular momenta associated with solutions which include shocks are not arbitrarily large. Rather, they are typically less than the marginally stable value  $l_{ms}$  as indicated in Fig. 3.

Global solutions which contain shock waves are not isolated solutions, but are present in a large range of energy and angular momentum. In Fig. 4, we show the variation of shock locations as a function of specific energy  $\mathcal{E}$ . Each set of curves, drawn for various specific angular momentum (marked on the set), consists of four segments: two for accretion ( $a_2 = r_{s2}$  and  $a_3 = r_{s3}$ ) and two for winds ( $w_2 = r_{s2}$  and  $w_3 = r_{s3}$ ). As discussed above,  $a_2$  and  $w_3$

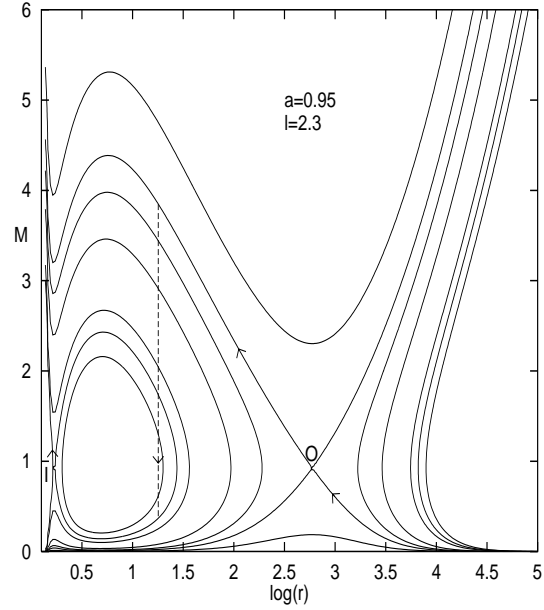


**Fig. 5a:** Example of shock transition in a prograde flow. The parameters are:  $a = 0.95$ ,  $l = 2.3$ ,  $\mathcal{E} = 1.001$ .

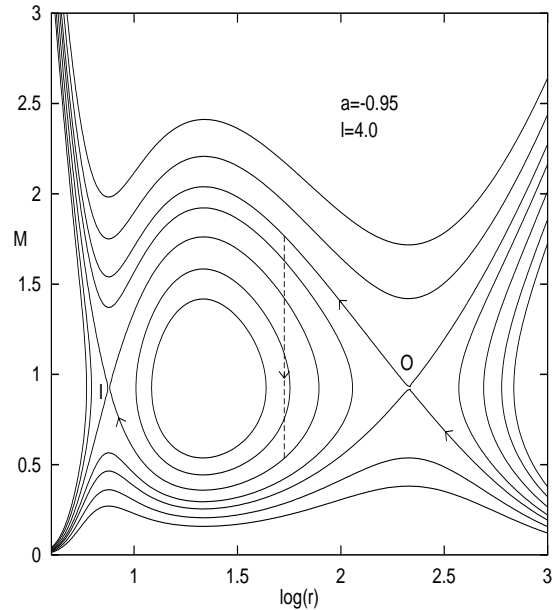


**Fig. 5b:** Example of shock transition in a retrograde flow. The parameters are:  $a = -0.95$ ,  $l = 4.0$ ,  $\mathcal{E} = 1.003$ .

(dotted curves) are unstable while  $a_3$  and  $w_2$  (solid curves) are stable. Kerr parameter  $a = 0.5$  is chosen. This example shows that stable shocks can form for a very wide class of flows. For corotating flows, the marginally stable and marginally bound angular momenta are  $l_{ms} = 2.9029$  and  $l_{mb} = 3.4142$  respectively. Thus the shocks form for angular momentum around these values. Since centrifugal barrier becomes stronger with angular momentum, shocks are located at larger radii for higher angular momenta. Another important point to note is that the shock location increases when the specific energy is increased. In a quasi-spherical flow, with the same input radial velocity and angular momentum, the potential energy decreases with height (since the gravity becomes weaker), thereby increasing the spe-

cific energy. Thus, shocks in a three-dimensional flow are expected to bend outwards. Such shocks have indeed been seen in numerical simulations of Hawley et al. (1984, 1985) and Molteni et al., 1996. Note that the parameters for stable shocks in accretion and winds are mutually exclusive. This is a consequence of the second law of thermodynamics, which requires that  $\dot{\mathcal{M}}_+ \geq \dot{\mathcal{M}}_-$  (C89).

We now compare the nature of shock solutions in prograde and retrograde flows. In Fig. 5a, we show a shock solution in prograde accretion with  $a = 0.95$ ,  $l = 2.3$ ,  $\mathcal{E} = 1.001$ . The eigenvalues of the entropy accretion rates at the outer ( $O$ ) and inner ( $I$ ) sonic points are,  $\dot{\mathcal{M}}_o = 2.973 \times 10^{-06}$ ,  $\dot{\mathcal{M}}_i = 4.108 \times 10^{-5}$  respectively and the stable shock is located at  $r_{s3} = 18.287$ . In Fig. 5b, we show a shock solution in retrograde accretion with  $a = -0.95$ ,  $l = 4.0$ ,  $\mathcal{E} = 1.0025$ . The eigenvalues of the entropy accretion rates at the outer ( $O$ ) and inner ( $I$ ) sonic points are,  $\dot{\mathcal{M}}_o = 1.097 \times 10^{-05}$ ,  $\dot{\mathcal{M}}_i = 1.478 \times 10^{-05}$  and  $r_{s3} = 53.41$ . For a retrograde flow, shock locations are generally higher than that for a prograde flow. Not shown in the figure is an interesting fact that the Mach number of the flow remains perfectly finite (typically in the range 5–8 in our examples) on the horizon.

#### 4 GLOBAL NATURE OF SHEAR TENSOR

In presence of viscosity, angular momentum transport is determined by the shear tensor. Whereas the computation of actual shear must be done in conjunction with the global solution of velocity components, presently we discuss its nature when the viscosity is weak, so that our inviscid global solution may be used instead. Around a Newtonian star, shear tensor component due to pure rotational motion can be defined as  $\sigma_{r\phi} = -rd\Omega/dr$  which is always positive ( $\sim 3/2\Omega$  for a Keplerian disk), and hence the viscous stress is always negative (that is why  $-\alpha P$  viscosity prescription of Shakura-Sunyaev [1973] was admissible). The viscous force in the  $\phi$  direction, caused by rubbing the adjacent layers generates a torque which would carry angular momentum only outwards. However, Anderson & Lemos (1988) pointed out that the shear can change sign near the horizon and they demonstrated this using velocity profiles of a cold radial flow below marginally stable orbit. Below we show that this conclusion remains similar for our global solution. It is to be noted that this shear is ‘passive’, namely, computed *after* the velocity profiles are known from our inviscid solution. On the other hand, this is certainly more accurate than what is obtained by rotational velocity alone. In presence of small viscosity, the behavior of our shear is expected to be the same. Computations with higher viscosities will be presented elsewhere.

In Section 2, we presented two definitions of shear tensor, one for the rotationally dominated flow and the other for the general flow. In Fig. 6, we compare these two definitions ( $\sigma_{\phi}^r|_{rot}$  and  $\sigma_{\phi\pm}^r$ ) using the velocity profiles from our solution. We also plot the gradient of angular velocity  $\Omega$  (dotted curve). The upper and lower panels are drawn using the parameters of Figs. 5a and 5b respectively. Thus they represent typical behaviours in prograde and retrograde flows respectively. We plot only the solution branches which pass through the outer sonic point (solid curve represents  $\sigma_{\phi+}^r$  for

the supersonic branch, and the long dashed curve represents  $\sigma_{\phi-}^r$  for the subsonic branch). The other branches which pass through the inner sonic point behave in a similar manner. Also shock-free global solutions show a similar behaviour. The difference in these two cases is due to significant radial velocity of the flow. We note that while the shear stress derived from rotational motion and that for the subsonic branch derived from general motion ( $\sigma_{\phi-}^r$ ) vanish on the horizon, the general shear on supersonic branch ( $\sigma_{\phi+}^r$ , which is relevant for our work) does not vanish on the horizon. This shows that a flow just outside the horizon will transport angular momentum towards the horizon. Although for any realistic viscosity, this behaviour is not expected to make any difference in the angular momentum distribution, and therefore our earlier computations (e.g. C90ab) which ignore such effect (by assuming  $\alpha P$  viscosity which is always positive, say) should remain valid. The reversal of the viscous stress is clearly due to the coupling of the rotational energy and the gravitational energy of the flow. Here, the ‘mass’ equivalent of the rotational energy is also attracted by gravity, making the attractive force stronger than that of a Newtonian star while the centrifugal force remains the same. The gravity always wins (giving rise to the well known ‘pit in the potential’ for any angular momentum). To remain in equilibrium the flow angular momentum must also rise as it approaches the black hole horizon and to achieve this the angular momentum must be transported inwards. This is the origin of the trend of the shear tensor. The non-linearity (coupling among all the energy terms) which gives rise to this interesting behaviour is the hall-mark of general relativity as is discussed in detail in Chakrabarti (1993).

#### 5 CONCLUDING REMARKS

In this paper we presented the equations governing a viscous transonic flow in vertical equilibrium around a Kerr black hole and obtained the complete set of global solutions of them. We showed that for a large region of the parameter space, a transonic flow can have a shock wave as well. We showed that standing shocks can form much closer to the black hole than shocks in the Schwarzschild geometry. This causes the post-shock region to be much hotter and may thus contribute to very high energy X-rays and  $\gamma$ -rays observed from black hole candidates (Chakrabarti & Titarchuk, 1995). Furthermore, the angular momentum required to have shock waves are also lower, (typically  $l \sim GM_{bh}/c$  for  $a \sim 1$ ) than that required for a Schwarzschild black hole (typically  $l \sim 4GM_{bh}/c$  for  $a = 0$ ). This is significant, as even with a small angular momentum the flow can have a stationary shock. It is true that the region of parameter space which forms a shock is limited, but numerical simulations (Molteni, Lanzafame & Chakrabarti, 1994; Molteni, Ryu & Chakrabarti, 1996) indicate that flows even outside this range of parameter contain shock waves, particularly because of the presence of turbulent pressure whose effects we have not included here.

Earlier (C89, C90ab, C96) our studies were made using pseudo-Newtonian potential, where the inner boundary, namely the horizon was not satisfactorily described. For instance, the angular velocity  $\Omega = l/r^2$  was not equal to the angular velocity on the horizon even for a Schwarzschild ge-



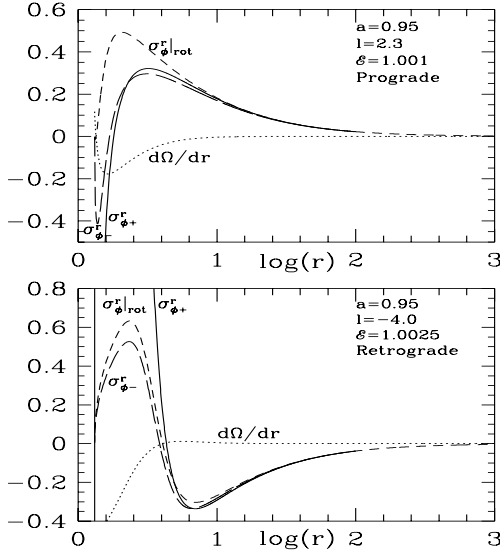


**Fig. 6:** Comparison of rotational shear stress  $\sigma_{\phi}^r|_{rot}$  (short dashed curves) with complete shear stress  $\sigma_{\phi+}^r$  (solid) along the supersonic branch (passing through outer sonic point) for (a) a prograde flow (upper panel) and (b) a retrograde flow (lower panel). Also shown is  $d\Omega/dr$  (dotted curves). For comparison, results of the subsonic branch ( $\sigma_{\phi-}^r$ ) which passes through the outer sonic point is also shown (long dashed). Note the change in sign of shear near the horizon.  $\sigma_{\phi+}^r$  does not vanish on the horizon, but  $\sigma_{\phi}^r|_{rot}$  and  $\sigma_{\phi-}^r$  do. Here, subscripts ‘+’ and ‘-’ denote supersonic and subsonic branches respectively.

ometry. Usually this was not a problem, since the potential energy was singular and the rotational energy due to any finite angular momentum was negligible compared to it. However, in our present analysis, such things do not arise. By definition,  $\Omega = u^{\phi}/u^t$  co-rotates with the horizon and our solution continuously or discontinuously extends from the horizon to infinity.

In this paper, we concentrated on the cases where the polytropic index  $n = 3$ , i.e.,  $\Gamma = 4/3$ . When the flow is completely gas pressure dominated, the flow may have  $\Gamma \sim 5/3$  in absence of cooling effects. In this extreme case, the flow will have only one (inner) saddle type sonic point (C90b) and the shocks can form only if the flow is already supersonic (e.g., when some wind is accreted). In reality, the flow will have intermediate polytropic index, dictated by cooling and heating processes and the possibility of shock formation will still be significant. The separation of topologies take place at around  $\Gamma = 1.5$  for flows in vertical equilibrium (C96).

We have discussed the behaviour of shear tensor components for our transonic solutions when the viscosity is negligible. Viscous stress shows a similar trend (namely, developing a maximum) as in a cold, radial flow (Anderson & Lemos 1988). However, unlike this case where the reversal occurs for a slowly rotating black hole, our hot, non-radial flow shows the trend of reversal even when the Kerr parameter

is high. The conclusions we drew for an inviscid flow cannot change dramatically when a weak viscosity is present, except that instead of ‘X’ and ‘O’ type sonic points, one will have ‘X’ and ‘spiral’ or ‘nodal’ type points (C90ab, C96). A flow which is cool and strictly Keplerian must be bound ( $\mathcal{E} < 1$ ) and therefore will not have shocks (Fig. 3) without additional energizing mechanism. The Keplerian disk will simply become sub-Keplerian due to pressure effects and enter through the inner sonic point before disappearing into the black hole. On the other hand, if the Keplerian disk is hot, and/or the sub-Keplerian flow originated from a cool Keplerian disk is re-energized (by magnetic flaring and other effects, for instance), or, if the sub-Keplerian flows are mixed with supersonic winds coming from companions then they can have standing shocks provided viscosity is below a critical value (C96). In fact, even in an axisymmetric fully three dimensional flow, in full Kerr geometry, the shocks form more easily above and below the equatorial plane (Chakrabarti, in preparation) where the accretion is presumably highly advective and sub-Keplerian. These considerations were used by Chakrabarti & Titarchuk (1995) to prove that the transition of spectral states of black hole candidates is due to variation of accretion rates. The analysis of 1100 days of BATSE data of Cyg X-1 (Crary et al, 1996) shows an excellent agreement with such considerations. In the absence of shocks, the spectral properties may vary similarly (our conclusions regarding the production of weak hard tail component in converging flows are independent of whether shocks form or not) since viscous effects (or, equivalently, accretion rates) change the transition radius where Keplerian disk becomes sub-Keplerian (C90ab; Chakrabarti & Titarchuk, 1995; C96). However, in this case variations in the hard and soft components are always correlated which are not observed in most of the black hole candidates, especially in wind fed systems. Thus, we believe two independent accretion components, namely, Keplerian and sub-Keplerian, should be present rather than one single component becoming sub-Keplerian and producing hard radiations. The most general solutions of advective disks in pseudo-Newtonian potential discussed these properties (C96) and we showed in the present paper that the general conclusions do not change even when the computations are carried out in full general relativity.

In the present paper, we have written the most general equations in Kerr geometry which govern hydrodynamics of the flow (originally attempted by NT73 in the Keplerian limit) by including radial velocity, and correcting the angular momentum transport equations with the use of conserved proper angular momentum and proper shear components. We already showed that the relevant shear components behave very differently from that of a flow around a Newtonian star. In future, we will present solutions of these equations for highly viscous flows.

The author thanks Kip Thorne and J. Peitz for discussion.

## REFERENCES

- Anderson, M.R. & Lemos, J.P.S 1988, MNRAS, 233, 489.  
 Bondi, H., MNRAS, 1952, 112, 195.  
 Chakrabarti, S.K. 1989, ApJ, 347, 365 [C89]

- Chakrabarti, S.K. 1990a, MNRAS, 243, 610 [C90a]  
Chakrabarti, S.K. Theory of Transonic Astrophysical Flows  
(World Scientific, Singapore, 1990b) [C90b]  
Chakrabarti, S.K. 1993, MNRAS, 261, 625  
Chakrabarti, S.K. & Molteni, D. 1993, ApJ, 417, 671  
Chakrabarti, S.K. & Titarchuk, L.G. 1995, ApJ, 455, 623.  
Chakrabarti, S.K. 1996, ApJ, 464, 664 [C96].  
Chakrabarti, S.K. 1996b, ApJ, in press.  
Crary, D.J. et al. ApJ, 1996, 462, 71L  
Flammang, R.A. MNRAS, 1982, 199, 833  
Hawley, J.F., Smarr L.L., & Wilson, J.R., 1984, ApJ, 277, 296  
Hawley, J.F., Smarr, L.L. & Wilson, J.R. 1985, ApJS, 55, 211  
Liang, E.P.T. & Thompson, K.A. 1980, ApJ, 240, 271  
Lynden-Bell, D. 1978, Phys. Scripta, 17, 185  
Molteni, D., Lanzafame, G. & Chakrabarti, S.K., 1994, ApJ, 425,  
161.  
Molteni, D., Ryu, D. & Chakrabarti, S.K., 1996, ApJ, in press.  
Moncrief, V., 1980, ApJ, 235, 1038  
Nakayama, K., 1994, MNRAS, 270, 871  
Nobuto, K. & Hanawa, T., 1994, PASJ, 46, 257  
Novikov, I. & Thorne, K.S., in: Black Holes, eds. C. DeWitt and  
B. DeWitt (Gordon and Breach, New York, 1973).  
Paczyński, B. & Wiita, P.J., 1980, A & A 88, 23.  
Peitz, J. Diplom Thesis, University of Heidelberg, 1994.  
Rees, M.J., Begelman, M.C., Blandford, R.D. & Phinney, E.S.,  
1982, Nature 295, 17.  
Ryu, D., Chakrabarti, S.K. & Molteni, D. 1997, ApJ, in press.  
Shakura, N.I. & Sunyaev, R.L., 1973, A & A, 24, 337.  
Shapiro, S.L. & Teukolsky, S.A., Black Holes, White Dwarfs and  
Neutron Stars — the Physics of Compact Objects (John Wi-  
ley & Sons, New York, 1983)  
Sponholz, H. & Molteni, D., 1994, MNRAS, 271, 233  
Wilson, J.R. 1978, ApJ, 173, 431

